The Isaac Newton Telescope Monitoring Survey of Local Group Dwarf Galaxies. V. The Star Formation History of Sagittarius Dwarf Irregular Galaxy Derived from Long-period Variable Stars

Tahere Parto[1,2], Shahrzad Dehghani[3], Atefeh Javadi[1], Elham Saremi[1,4,5], Jacco Th. van Loon[6], Habib G. Khosroshahi[1,7], Iain McDonald[8], Mohammad T. Mirtorabi[2], Mahdieh Navabi[9], and Maryam Saberi[10,11]

[1] School of Astronomy, Institute for Research in Fundamental Sciences (IPM), P.O. Box 1956836613, Tehran, Iran; atefeh@ipm.ir
[2] Physics Department, Alzahra University, Vanak, 1993891176, Tehran, Iran
[3] Department of Physics, University of Cologne, Cologne, Germany
[4] Instituto de Astrofísica de Canarias, Vía Láctea s/n, E-38205 La Laguna, Tenerife, Spain
[5] Departamento de Astrofísica, Universidad de La Laguna, E-38205 La Laguna, Tenerife, Spain
[6] Lennard-Jones Laboratories, Keele University, ST5 5BG, UK
[7] Iranian National Observatory, Institute for Research in Fundamental Sciences (IPM), Tehran, Iran
[8] Jodrell Bank Centre for Astrophysics, Alan Turing Building, University of Manchester, M13 9PL, UK
[9] School of Astronomy, Institute for Research in Fundamental Sciences (IPM), P.O. Box 1956836613, Tehran, Iran
[10] Rosseland Centre for Solar Physics, University of Oslo, P.O. Box 1029 Blindern, NO-0315 Oslo, Norway
[11] Institute of Theoretical Astrophysics, University of Oslo, P.O. Box 1029 Blindern, NO-0315 Oslo, Norway

Abstract

We conducted an optical monitoring survey of the Sagittarius dwarf irregular galaxy (SagDIG) during the period of 2016 June–2017 October, using the 2.5 m Isaac Newton Telescope at La Palama. Our goal was to identify long-period variable stars (LPVs), namely, asymptotic giant branch stars (AGBs) and red supergiant stars, to obtain the star formation history of isolated, metal-poor SagDIG. For our purpose, we used a method that relies on evaluating the relation between luminosity and the birth mass of these most evolved stars. We found 27 LPV candidates within 2 half-light radii of SagDIG. 10 LPV candidates were in common with previous studies, including one extreme-AGB (x-AGB). By adopting the metallicity $Z = 0.0002$ for older populations and $Z = 0.0004$ for younger ages, we estimated that the star formation rate changes from 0.0005 ± 0.0002 $M_\odot$ yr^{-1} kpc^{-2} (13 Gyr ago) to 0.0021 ± 0.0010 $M_\odot$ yr^{-1} kpc^{-2} (0.06 Gyr ago). Like many dwarf irregular galaxies, SagDIG has had continuous star formation activity across its lifetime, though with different rates, and experiences an enhancement of star formation since $z \simeq 1$. We also evaluated the total stellar mass within 2 half-light radii of SagDIG for three choices of metallicities. For metallicity $Z = 0.0002$ and 0.0004, we estimated the stellar mass $M_* = (5.4 \pm 2.3) \times 10^6$ and $(3.0 \pm 1.3) \times 10^6$ $M_\odot$, respectively. Additionally, we determined a distance modulus of $\mu = 25.27 \pm 0.05$ mag, using the tip of the red giant branch.

Unified Astronomy Thesaurus concepts: Dwarf galaxies (416)

1. Introduction

The physical properties of dwarf galaxies make them excellent objects for studying the formation and evolution of galaxies. They are the most dark matter-dominated galaxies and the simplest systems that demonstrate how dark matter works on small scales. Furthermore, they are located at extreme limits for the formation of galaxies in terms of size, mass, and metallicity Simon (2019). The internal and environmental mechanisms can severely affect these low-mass systems, which can be studied to determine the role of different processes and their efficiencies in the evolution of galaxies (Haynes 2019). Among the different morphologies of dwarf galaxies, dwarf irregulars (dIrrs) are typically gas-rich. They can be used to investigate the relation between stellar and gas-phase metallicities to see how gas flows shape the metallicity distribution and to what extent the high gas fraction can affect their metallicities (Kirby et al. 2017). They are also key to answering questions such as the efficiency of star formation in low gas densities, the importance of sequential star formation, and the

possible role of star formation in creating breaks in the structure of the outer regions of spiral galaxies (Hunter et al. 2012). Low-metallicity dIrrs resemble the building blocks of the universe and reveal the efficiency of different astrophysical processes in forming the first stars. Moreover, they help in trying to figure out questions about dust formation in the early universe (e.g., Boyer et al. 2014).

The Local Group (LG) offers advantages to the study of dwarf galaxies due to their proximity and their range in mass, morphology, and age. Among LG dwarfs, the Sagittarius dwarf irregular galaxy (SagDIG) has unique features that make understanding its formation history a topic of high interest. The first and foremost feature is its low metallicity $Z = 0.00025$ (Momany et al. 2002). Combined with its close distance 1.07 ± 0.09 Mpc (Momany et al. 2002), it allows for finding resolved metal-deficient stars. The other particular property of SagDIG is its notable gas fraction, $M(\text{H I})/M_* = 4.6 \pm 1.2$ (Kirby et al. 2017). It leads to a high star formation rate (SFR), making SagDIG the most rapidly growing galaxy among LG dwarf galaxies (Kirby et al. 2017). Moreover, the isolation of SagDIG makes it an ideal laboratory to study how a low-mass galaxy would evolve in the absence of environmental effects (Weisz et al. 2014).

SagDIG was found by Cesarsky et al. ([1978](#)) and Longmore et al. ([1978](#)) with the 1 m ESO Schmidt telescope and through the UK Schmidt IIIaJ Southern Sky Survey, respectively. Later inspections of this object revealed its irregular shape (Cesarsky et al. [1978](#); Longmore et al. [1978](#)). Various studies calculate its distance modulus using the tip of red giant branch stars (TRGBs). To name a few, Momany et al. ([2002](#)) found the distance modulus of $\mu = 25.14 \pm 0.18$ mag, Weisz et al. ([2014](#)) estimated $\mu = 25.11$ mag, and Higgs et al. ([2016](#)) estimated $\mu = 25.36 \pm 0.15$ mag. In this study, we adopted $\mu = 25.27 \pm 0.05$ mag, which we estimated using the method in Section [4](#).

The star formation history (SFH) of SagDIG has been estimated in many studies. Karachentsev et al. ([1999](#)) estimated the SFH of SagDIG by classifying and counting stars in the young and old populations based on their color and position on an [I, V–I] color–magnitude diagram (CMD) and employing a synthetic CMD. They found that SagDIG has an ongoing star formation similar to other dIrrs such as NGC 6822, Pegasus, Sextans A, and Antlia with a rate 10 times higher than the average of its entire lifetime SFR.

Momany et al. ([2005](#)) used Hubble Space Telescope/ Advanced Camera for Surveys (HST/ACS) deep images and identified a well-populated RGB. They concluded that the main population of this galaxy are stars older than 1 Gyr. They also found populations of main-sequence stars, He-burning blue loop stars, blue and red supergiants (RSGs), and a population of AGBs that show extended star formation in this galaxy. Moreover, using the luminosity function of main-sequence stars, they estimated an SFR for the last few hundred megayears and concluded that the SFR is mainly constant in this time interval. Weisz et al. ([2014](#)) used HST archival images to study the SFHs of 40 LG galaxies, including SagDIG. They constructed a model CMD for each galaxy and matched it to the observed CMD to derive the cumulative SFH with random and systematic errors. We compare our results with these studies in Section [6](#).

It is also possible to investigate the history of a galaxy with long-period variable stars (LPVs), namely, AGBs and massive RSGs. LPVs are the most evolved stars with strong radial pulsation due to variations in the opacity and radiation transport, leading to a fluctuation in their brightness within 300–1200 days. Although different types of variable stars could be beneficial for the aim of the SFH survey, the use of LPVs is more advantageous. First, LPVs are at the last stage of evolution, and the relation between stars' luminosity and birth mass can be applied to estimate an LPV's mass. Second, LPVs cover a diverse range of ages between 30 Myr and 10 Gyr old. Third, LPVs' brightness in the near-infrared is less affected by circumstellar extinction (Javadi et al. [2011a](#), [2011b](#)).

This work is part of the Isaac Newton Telescope monitoring survey of LG dwarf galaxies. Various types of dwarf galaxies, including 43 dwarf spheroidals, six dIrrs, six dwarf transition galaxies, and four globular clusters come under the scrutiny of our team (Saremi et al. [2017](#); Parto et al. [2021](#)). The main objectives of this survey include identifying all LPVs in the dwarf galaxies of the LG observable in the northern hemisphere; obtaining accurate time-averaged photometry for all LPVs; constructing the SFHs from LPVs luminosity distribution; obtaining their pulsation amplitude; modeling their spectral energy distributions; and studying their mass loss as a function of stellar properties such as mass, luminosity,

Table 1
Log of WFC Observations of SagDIG

Date (y/m/d)	Epoch	Filter	t_{exp} (s)	Seeing arcsec	Airmass
2016/6/13	1	i	719	2.61	1.711
2016/8/10	2	i	555	1.23	1.564
2016 8/10	2	V	735	1.64	1.471
2016/8/12	2	i	558	1.37	1.449
2016/10/21	3	i	2715	1.84	1.595
2017/8/2	4	i	555	1.44	1.453
2017/8/2	4	V	735	1.37	1.450
2017/9/2	5	i	555	1.08	1.457
2017/9/2	5	V	735	1.18	1.449
2017/10/6	6	i	555	1.61	1.511
2017/10/8	6	V	735	1.82	1.542

metallicity, and pulsation amplitude (Saremi et al. [2020](#)). This paper (paper V) focuses on constructing the SFH of SagDIG. Paper I (Saremi et al. [2020](#)) introduced the survey and the detection of LPVs in Andromeda I (And I), Paper II (Saremi et al. [2021](#)) presents the results of the SFH of And I. Paper III (in preparation) discusses the role of LPVs in the chemical enrichment of And I, and paper IV (Navabi et al. [2021](#)) presents the SFH of Andromeda VII (And VII).

This paper is organized as follows: In Section [2](#), we describe observations, data reduction, photometry, and contamination. We also compare our catalog with previous catalogs of SagDIG. In Section [3](#), we present a method to find LPVs. In Section [4](#), we estimate the distance modulus using the TRGB method. In Section [5](#), we introduce the method we use for constructing the SFH. In Section [6](#), we discuss our results, followed by a summary and conclusions in Section [7](#).

## 2. Observation and Data Processing

Images of SagDIG in the i and V bands were obtained from 2016 June–2017 October using the Isaac Newton Telescope (INT) Wide Field Camera (WFC), which includes four CCDs with 4100×2046 pixel dimension and a pixel scale of $0''\!.33$. The observing log is presented in Table [1](#). In Figure [1](#), the master image in the i and V bands, restricted to a field of $10' \times 6'$, is presented. The coordinate center of SagDIG is located in the center of the central CCD (CCD 4). Since more than twice the half-light radii of SagDIG are covered in CCD 4, we only considered this CCD for the photometry procedure.

The WFC images were reduced by the THELI image processing pipeline (Erben et al. [2005](#)). We performed the photometry process in both filters using the DAOPHOT package (Stetson [1987](#)). For this purpose, we used the DAOPHOT routine to select 40 isolated stars in different positions on the field and built a constant point-spread function (PSF) model for each image. A master image was made by combining single images (using DAOMATCH, DAOMASTER, and MONTAGE2 routines) to generate a star list (using the ALLSTAR routine). The ALLFRAME routine uses the star list to estimate the instrumental magnitudes of stars by fitting the PSF models in individual images (Stetson [1994](#)).

The transformation of the instrumental magnitudes onto the standard system was carried out using observations of standard stars (Landolt [1992](#)), and the NEWTRIAL routine (Stetson [1996](#)). The final catalog consists of 12,538 stars in the field of CCD 4 and 678 stars in the $2r_h$ from the center of SagDIG, assuming the half-light radius $r_h = 1'\!.1$ (Beccari et al. [2014](#)). Additional
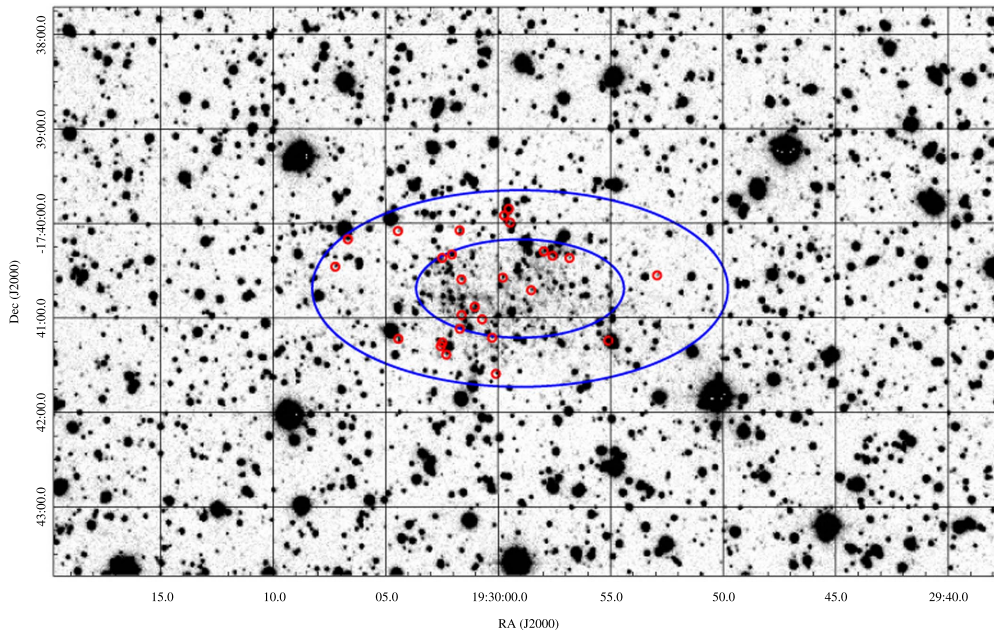
Figure 1. The master WFC image of SagDIG galaxy restricted to a field of $10' \times 6'$. The LPV candidates are marked with red circles. Blue ellipses show the half and 2 half-light radii of SagDIG (Beccari et al. 2014), with an ellipticity of 0.50 and a position angle of $90°$ (McConnachie 2012).
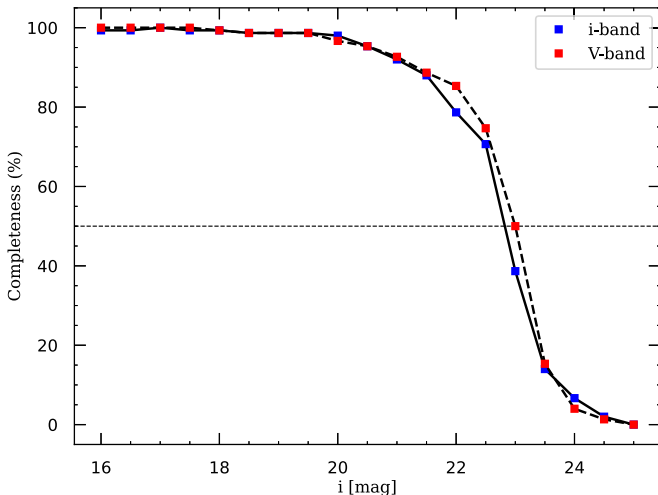
Figure 2. Completeness as a function of i- and V-band magnitudes. The photometry completeness level is 50% for stars with $i \approx 23$ mag.

details on the observations and photometry procedures are provided in Saremi et al. (2020).

The process of adding 2550 artificial stars was carried out to evaluate the completeness of the survey, using the ADDSTAR task (Stetson 1987), in both i- and V-band single frames, in 17 discrete 0.5 magnitude bins started from 16–24.5 mag. The fraction of recovered artificial stars is estimated by the ALLFRAME task. As shown in Figure 2, our survey is sufficiently complete up to 22 mag in the i and V bands, near the TRGB (Section 4). Moreover, it is up to 50% complete for stars with magnitude ≈ 23 mag in both filters, which affirms that nearly the entire AGBs and RSGs are detected for our purpose.

2.1. Calibration

Different corrections were applied to the stars' magnitude, including aperture correction (by choosing 50 stars with good photometry to calibrate the PSF-fitting photometry using

DAOGROW (Stetson 1990), COLLECT (Stetson 1993), and NEWTRIAL routines), photometric correction (by applying atmospheric extinction correction and zero-points derived from the photometry of standard star images), and relative calibration (Saremi et al. 2020). To perform the relative calibration of all images corresponding to one another, we selected 4434 mutual stars with $i \in [19.0, 22.0]$ mag. The average magnitude of these chosen stars was taken as the calibration value, and it varies by -0.01 to 0.03 mag.

In the end, to examine the precision of our estimated magnitudes and the applied calibrations, we crossmatched our catalog with previous surveys. Here, we present our results for the Pan-STARRS release 1 (PS1) Survey (Chambers et al. 2016), in the i band and Beccari et al. (2014) for the V band. Figure 3 shows good accordance up to $i = 22$ mag between our photometry and the two other surveys. For fainter stars, differences increase but as far as we are concerned with AGB and RSG stars, our survey is good enough for our purpose.

3. Variability Analysis

In order to find LPV stars, we employed the same method presented in Stetson (1996) to calculate the variability index L given in Equation (1):
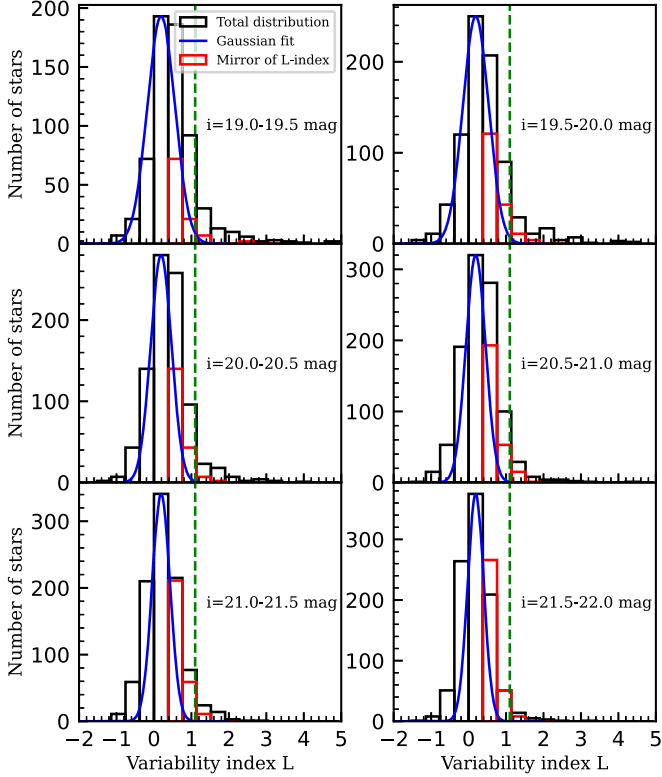
$$L = \left(\frac{J \times K}{0.798} \right) \left(\frac{\sum_{i=1}^{N} w_i}{w_{\text{all}}} \right), \tag{1}$$

where the K index is the kurtosis of the magnitude distribution and the J index is defined for n pairs of observations in different or same filters that are on the same night or in a time interval much smaller than the periodicity of LPVs. For variable stars, J has a positive and significant value compared to the non-variables and is calculated as

$$J = \frac{\sum_{K=1}^{N} w_k \, \text{sign}(P_K) \sqrt{|P_K|}}{\sum_{K=1}^{N} w_k}, \tag{2}$$
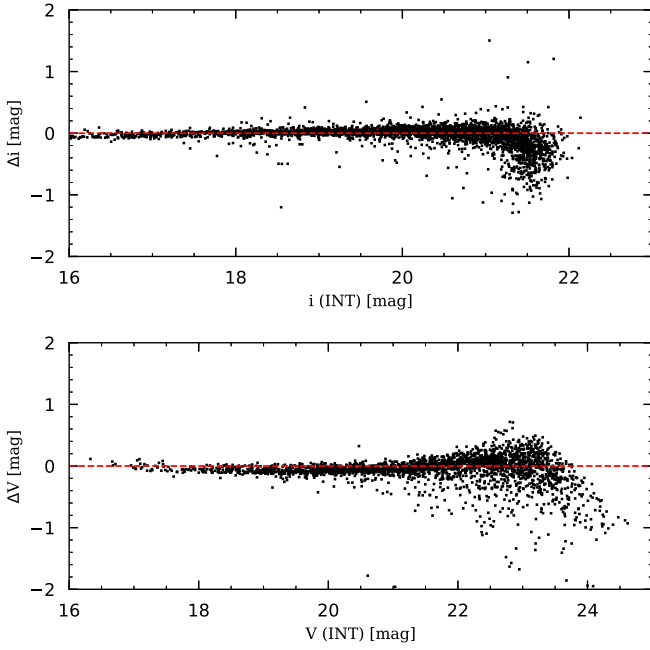
Figure 3. Difference between the magnitude of stars in our catalog and Chambers et al. (2016) for the *i* band and Beccari et al. (2014) for the *V* band.

Figure 4. Histogram of the variability index *L* vs. magnitude for a 19–22 mag interval, fitted by the Gaussian function (in blue). The left side of the maximum are non-variable stars, and the red bins show a mirror of their distribution. Green-dashed lines depict the $L = 1.1$ variability index threshold.
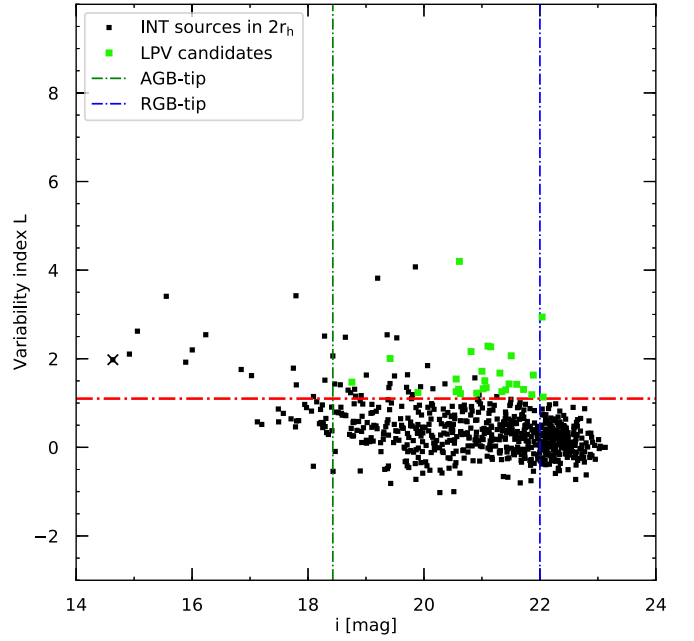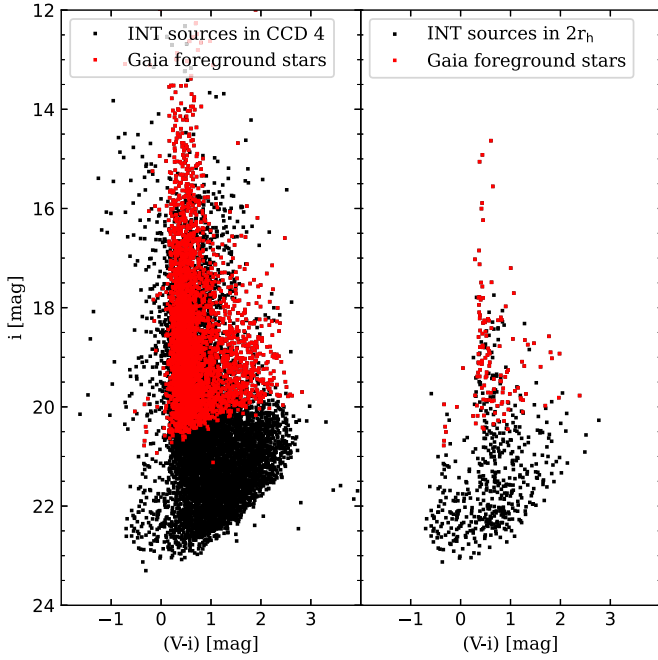

Figure 5. Variability index *L* vs. *i*-band magnitude. INT sources and LPV candidates within two half-light radii from the center of SagDIG are shown in black and green, respectively. The red horizontal line at $L = 1.1$ indicates the chosen threshold for variable identification. The AGB tip and RGB tip are shown in green and blue dashed lines, respectively. The black cross is a non-variable source with a large RUWE parameter (see Section 3.1).

Figure 4 shows histograms of variability index *L* versus *i*-band magnitudes in six magnitude bins in a range that covers the AGB tip and RGB-tip interval. Stars with negative *L* are non-variables and located at the left side of the maximum ($L \simeq 0$). We expect that non-variable stars form a normal distribution, as they are dominant in number. Hence, we fitted a Gaussian function to the left side of the distribution; the positive part of this fit is assumed to trace the distribution of non-variable stars. We defined a threshold for the variability index *L* where the ratio of Gaussian fit to actual distribution has diminished to 0.1. This means that 90% of the variable stars in the deviation part of the distribution are selected accurately, and only 10% might be non-variables. We located the variability index threshold at $L = 1.1$, which is shown by vertical green-dashed lines in Figure 4.

Applying $L \geqslant 1.1$, we found 2539 LPV candidates in the CCD 4 and 70 within 2 half-light radii of SagDIG. We visually examined all the LPV candidates to trace a possible negative correlation with the magnitude changes of a bright neighbor. Figure 5 shows the variability index of all sources within 2 half-light radii of the galaxy versus stellar magnitude. Genuine LPV candidates are shown as green dots. It is noticeable that they occupy the magnitude interval between the AGB tip and RGB tip. There are also sources with $L > 1.1$ but marked with black dots as non-variable stars. Nearly all of these sources have magnitudes greater than 20 mag. They are either foreground contamination (as discussed in Section 3.1) or blended by a bright neighbor, making their estimated index *L* unreliable.

3.1. Foreground Contamination

SagDIG with $l = 21°054$ and $b = -16°288$ is projected near the center of the Milky Way, and the observation of the field is

where P_K is the normalized magnitude residuals of two paired observations (Stetson 1996). *w* is the weight parameter set to 1 for a paired observation and to 0.5 for a single observation. *N* is the number of observations, and w_{all} is the total weight of a star.
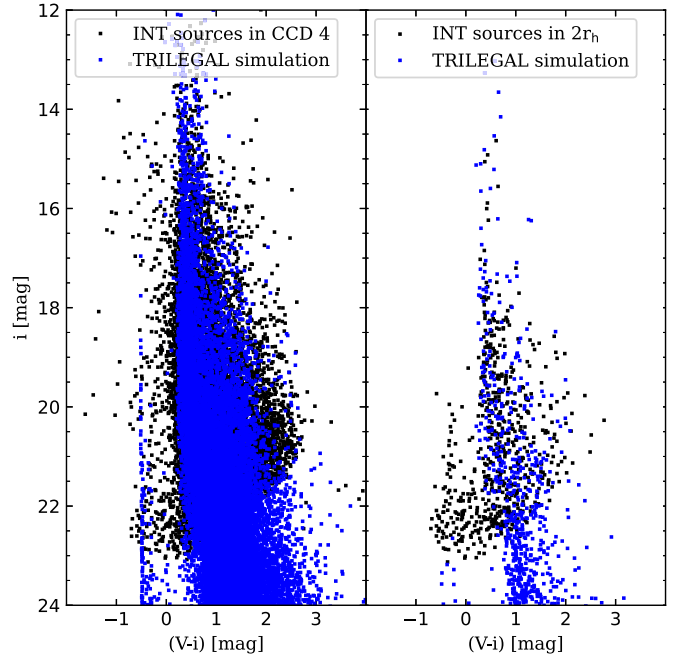
Figure 6. The foreground contamination in the line of sight to SagDIG shown by red dots, obtained by imposing conditions on the Gaia DR3 catalog (Gaia Collaboration et al. 2021). Left: stars across CCD 4. Right: stars within $2r_h$ from the center of SagDIG.

Figure 7. The foreground contamination in the line of sight to SagDIG, obtained with the TRILEGAL simulation (Girardi et al. 2005) represented as blue dots. Left: stars across CCD 4 ($\simeq 0.07$ deg^2). Right: stars within $2r_h$ from the center of SagDIG ($\simeq 0.002$ deg^2).

negatively influenced by the heavy foreground contamination. To have a reliable list of LPV candidates, we crossmatched our catalog with that of the Gaia DR3 Gaia Collaboration et al. (2021) and imposed the constraints described in Saremi et al. (2020) on the proper motion and parallax of Gaia stars. Gaia DR3 also provides a new parameter RUWE (renormalized unit weight error) that identifies spurious sources.

In total, we found 3418 foreground stars in CCD 4 and 132 ones inside $2r_h$ from the center of SagDIG, including 15 stars from our LPV candidates. Among these 15 stars, only one has a RUWE parameter larger than 1.4, suggesting it may be a binary star or a star with a disturbing neighbor (Gaia Collaboration et al. 2021). We marked it with a cross in Figure 5.

As Figure 6 shows, Gaia DR3 covers only the upper part of the CMD. Hence, it provides no counterparts for stars with a magnitude fainter than $i \simeq 20.5$ mag. To examine the density of foreground contamination and compare it to Gaia DR3 coverage, we used the TRILEGAL population synthesis code (Girardi et al. 2005), with the Galactic halo, bulge, thin, and thick disk components and by applying V-band extinction $A_V(\infty) = 0.338$ mag. Figure 7 shows the simulated contamination in the line of sight to SagDIG in blue dots, for the entire CCD 4 ($\simeq 0.07$ deg^2, left) and for $2r_h$ from the center of SagDIG ($\simeq 0.002$ deg^2, right). Across the CCD 4 and for $i < 20.5$ mag, TRILEGAL estimated 4277 contamination sources, while Gaia DR3 suggested 3395. Likewise, inside $2r_h$, TRILEGAL and Gaia DR3 estimated 137 and 129 sources, respectively. The estimation ratio shows that Gaia coverage for $i < 20.5$ mag is acceptable, especially within $2r_h$, which is crucial in our study.

To assess the contamination for $i > 20.5$ mag, we compared our catalog and TRILEGAL estimation of the stellar surface density. For this purpose, we only considered stars in an area in the CMD where we most expect the LPVs ($18.4 < i < 22$, $0 < V - i < 3$ mag), though with a lower magnitude limit of

20.5 mag. We measured the stellar surface density inside $2r_h$ and the entire CCD 4 of 0.008 and 0.003 arcsec^{-2}. In comparison, TRILEGAL estimated the foreground density in these regions at 0.0001 and 0.004 arcsec^{-2}, respectively. Although the contamination level across the CCD 4 is significant, within $2r_h$ and in our considered color and magnitude intervals, it is negligible.

In the end, 27 stars remained as our final LPV candidates. We omitted 28 sources with corrupted profiles from the initial list due to blending caused by bright neighbors (see Section 3), and 15 stars were among the foreground contamination. The photometric properties of the LPV candidates can be found in Table 2.

3.2. LPV Candidates and the CMD

Figure 8 shows the LPV candidates within 1 and 2 half-light radii of the galaxy. The PARSEC−COLIBRI (Marigo et al. 2017) isochrones with $Z = 0.00025$ and our estimated distance modulus in Section 4 are overplotted. The RGB tip (Section 4) and AGB tip are presented in magenta-dashed lines. Nearly all LPV candidates are brighter than the RGB tip, as we expected. We estimated the theoretical AGB tip using the classical core −luminosity relation. The absolute bolometric magnitude for a Chandrasekhar core mass is ≈ -7.1. For SagDIG metallicity and distance modulus, the $\log(t[\mathrm{Gyr}]) = 8.0$ isochrone reaches this value at $i = 18.43$ mag.

The amplitude of a sinusoidal light curve, similar to a variable star's light curve, is obtained by $A = 2\sigma\,0.707^{-1}$, where σ is the standard deviation of the stellar magnitudes. As shown in Figure 9, the amplitude of stars is between 0.16 and 1.8 mag, and stars with higher amplitude appear dimmer (left panel). The horizontal red line shows a threshold of 0.2 mag for the amplitude of the pulsation. Stars with lower amplitude tend to be RSG stars (Javadi et al. 2011a).

Table 2
Photometric Properties of the Detected LPV Candidates in SagDIG

| ID	R.A. (J2000)	Decl. (J2000)	V	err_V	i	err_i	n[a]	m[b]	J Index	K Index	L Index	Amplitude
5129	19:30:04.424	−17:40:04.54	22.744	0.1420	21.718	0.0668	3	7	1.111	0.918	1.306	0.588
5131	19:30:04.407	−17:41:12.93	22.597	0.2485	21.409	0.1556	3	7	0.994	0.757	1.297	1.437
5408	19:30:02.520	−17:41:17.53	21.757	0.1950	21.073	0.0975	4	6	1.413	0.660	1.347	0.584
5415	19:30:02.460	−17:40:21.59	22.460	0.2600	21.600	0.0866	3	7	1.627	0.715	1.422	0.674
5420	19:30:02.453	−17:41:15.33	22.074	0.2926	21.310	0.1117	4	7	1.536	0.597	1.676	0.784
5444	19:30:02.278	−17:41:22.98	21.674	0.2052	21.000	0.1062	1	7	1.796	0.660	1.717	1.211
5514	19:30:02.026	−17:40:19.41	19.722	0.0183	19.416	0.0150	4	7	2.078	0.821	2.005	0.157
5560	19:30:01.683	−17:40:04.14	21.972	0.1131	20.611	0.1020	4	7	3.153	0.616	4.197	0.596
5562	19:30:01.675	−17:41:06.57	22.666	0.2053	21.151	0.1093	3	7	2.202	0.798	2.270	0.719
5578	19:30:01.606	−17:40:35.25	23.169	0.2034	21.344	0.0666	1	7	0.901	0.806	1.257	0.424
5580	19:30:01.594	−17:40:57.83	22.204	0.1967	21.860	0.1718	4	7	0.468	0.627	1.188	1.195
5699	19:30:01.015	−17:40:52.63	22.394	0.1176	20.629	0.0390	4	7	1.247	0.679	1.213	0.313
5749	19:30:00.687	−17:41:00.56	99.999	9.9999	22.038	0.2991	0	6	3.593	0.699	2.942	1.801
5808	19:30:00.241	−17:41:12.25	21.499	0.0783	21.050	0.0707	4	7	1.434	0.680	1.503	0.558
5831	19:30:00.072	−17:41:35.17	23.003	0.1206	21.021	0.0946	2	7	1.350	0.602	1.322	0.574
5865	19:29:59.766	−17:40:34.08	22.333	0.1022	20.555	0.0352	4	7	1.273	0.758	1.256	0.275
5875	19:29:59.708	−17:39:54.65	21.272	0.1519	20.812	0.1451	1	6	2.176	0.599	2.162	0.991
5909	19:29:59.442	−17:39:59.22	22.345	0.3693	21.886	0.1294	3	7	1.383	0.833	1.631	0.927
6092	19:29:58.505	−17:40:42.12	21.966	0.1130	21.468	0.0712	4	7	1.437	0.828	1.431	0.538
6161	19:29:57.944	−17:40:17.46	21.311	0.1018	20.597	0.1429	4	7	0.089	0.514	1.313	0.927
6217	19:29:57.553	−17:40:20.30	22.042	0.2068	21.505	0.1372	4	7	1.205	0.617	2.067	0.790
6941	19:29:52.909	−17:40:32.73	23.020	0.2469	21.103	0.0769	3	7	1.922	0.720	2.285	0.497
6345	19:29:56.801	−17:40:21.69	22.635	0.1134	22.057	0.1027	4	7	1.133	0.694	1.135	0.689
4727	19:30:07.209	−17:40:27.10	23.399	0.3766	20.910	0.0523	2	7	1.144	0.806	1.223	0.351
4822	19:30:06.648	−17:40:09.73	21.084	0.1367	20.556	0.0933	4	7	1.789	0.662	1.542	1.158
6578	19:29:55.074	−17:41:14.11	19.438	0.3179	18.757	0.2712	4	6	1.088	0.844	1.471	1.541
5900	19:29:59.500	−17:39:50.48	20.425	0.0462	19.896	0.1353	4	7	1.067	0.658	1.236	0.744

Notes.
[a] n is the number of observations in the V band.
[b] m is the number of observations in the i band.
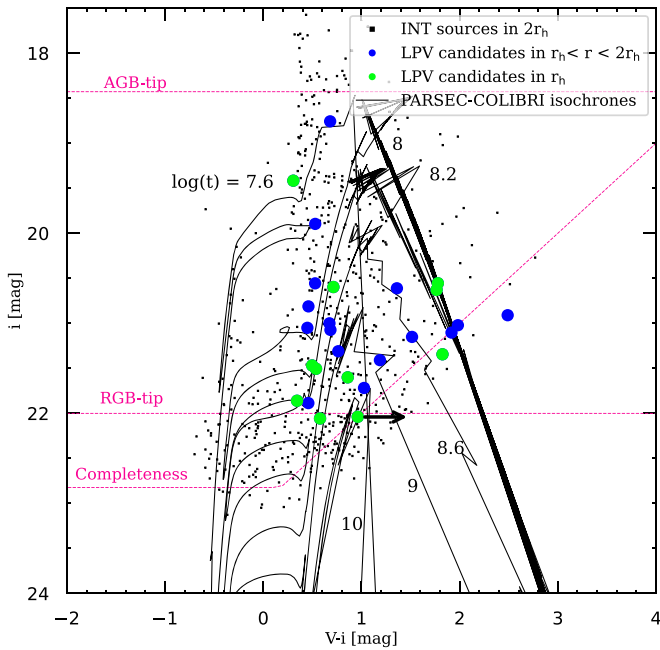
Figure 8. CMD of stars within $2r_h$ of SagDIG along with the PARSEC −COLIBRI isochrones. Green dots denote LPV candidates inside of $r_h = 1.''1$, and blue dots denote LPV candidates inside $r_h < r < 2r_h$. The AGB tip, RGB tip, and completeness limit are shown in magenta-dashed lines. The black arrow shows the lower limit for the color of the LPV candidate ID = 5749.
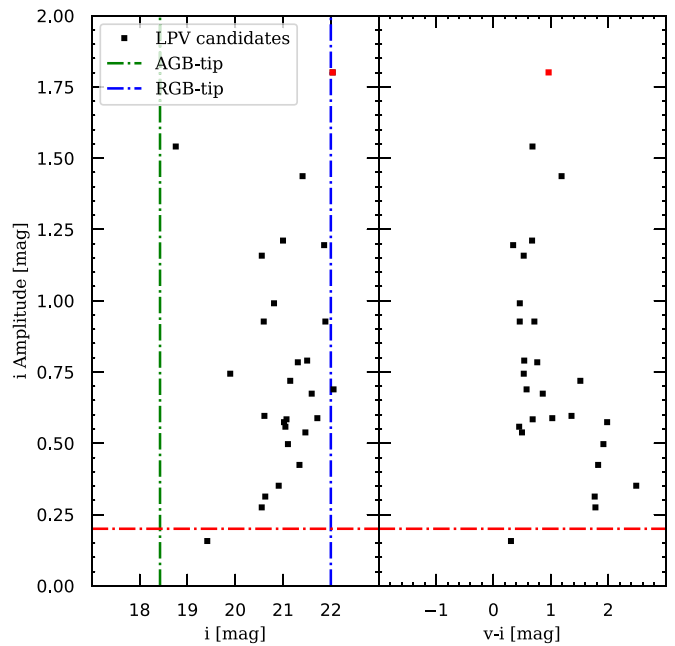
Figure 9. The estimated amplitude of LPV candidates vs. magnitude (left panel) and color (right panel). The red line $A_i = 0.2$ mag separates RSGs from AGBs. The blue- and green-dashed lines in the left panel represent the RGB tip and AGB tip, respectively. The red dot denotes the largest amplitude $A_i = 1.80$ mag, and its light curve is shown in the bottom panel of Figure 10.
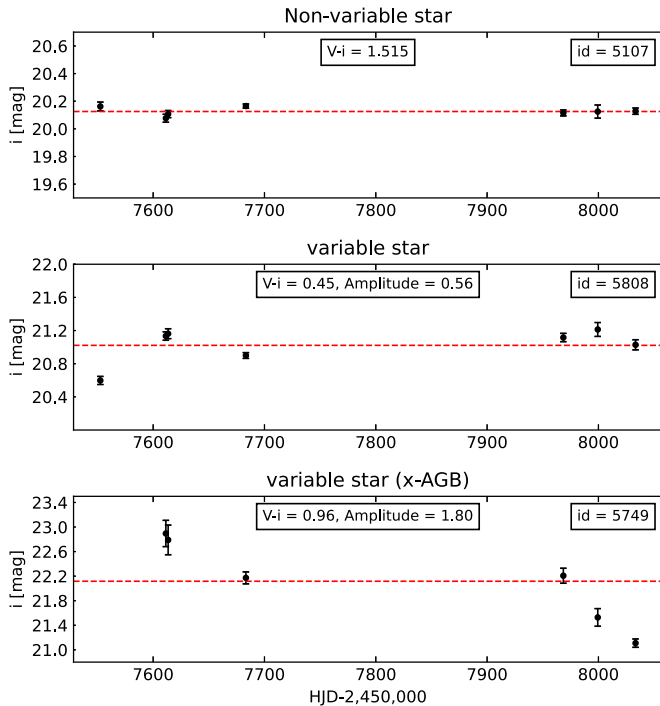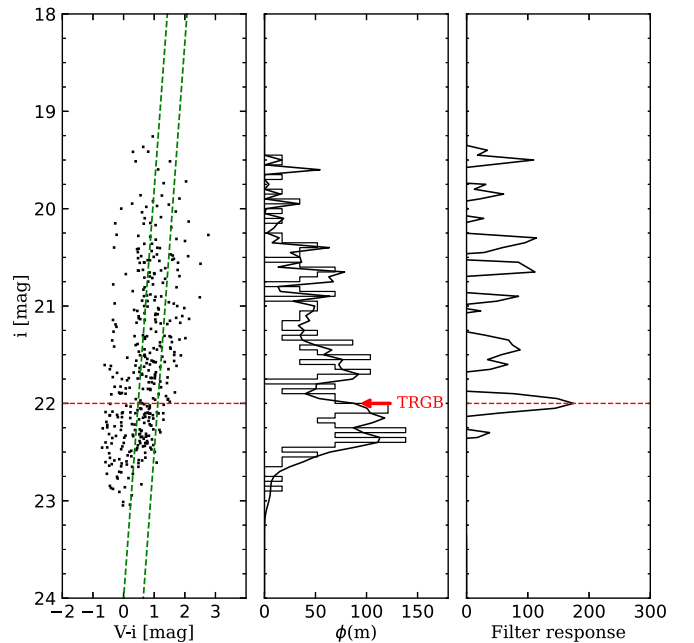
Figure 10. Light curve of a typical non-variable star with the color term (upper panel). The light curve of a variable star with moderate amplitude (middle panel). The light curve of a variable star (x-AGB; see Section 6.2) with strong pulsation and high amplitude (bottom panel).

Figure 11. Left panel: the CMD within $2r_h$ radii of SagDIG. Stars between green tramlines were employed to detect the TRGB. The red-dashed line shows the i-magnitude of the TRGB for SagDIG. Middle panel: the smoothed luminosity function $\phi(m)$ overplotted on the luminosity function histogram with a binning width of 0.05. Right panel: the output of the edge detection using a Sobel kernel.

In Figure 10, the light curves of a non-variable star and two LPV candidates are shown. ID = 5749 is an x-AGB star (Section 6.2) and has the largest amplitude (1.8 mag). Due to limited observation nights, we cannot calculate the period of LPVs precisely, but the color of LPVs correlates with their amplitude and period. Among our LPV candidates, ID = 5749 is not visible in the V band; hence, we considered the completeness limit of 50% in the V band as its magnitude. The black arrow in Figure 8 indicates this star's lower color term limit. Using the Spitzer data in Section 6.2, we found the color term $i - [3.6] = 6.03$ mag for this star, which shows x-AGBs produce a large amount of dust and supports the strong relation of color with amplitude and pulsation.

4. Distance Estimate by Locating the TRGB

The TRGB is the point where low-mass stars reach their highest luminosity due to the helium flash in their degenerate helium core. At this point, the infrared magnitude (usually the I band) of stars has a slight dependence on metallicity and age Lee et al. (1993), and can be used as an extragalactic distance indicator. The TRGB as a standard candle has some advantages over other distance estimators such as RR Lyrae and Cepheid stars. The magnitude of TRGBs is brighter than that of RR Lyrae stars, and compared to Cepheids, the TRGB is less affected by extinction. Nevertheless, the presence of AGB stars near the tip of an RGB can make TRGB detection problematic in some cases (Lee et al. 1993).

We used the Sakai et al. (1996) Gaussian smoothed luminosity function $\phi(m)$ and a Sobel kernel $[-2, -1, 0, 1, 2]$ to perform edge detection. In order to only include RGB stars, we restricted stars within $2r_h$ of SagDIG with colors between the green tramlines, as shown in Figure 11. We found the i-band magnitude of the TRGB equal to 22.00 ± 0.05 mag

for SagDIG (red-dashed line in Figure 11). To estimate the distance modulus from the i band, we used the luminosity of the TRGB in the i band, $i_0 = 3.53$ mag (Higgs et al. 2016), and adopted the i-Sloan correction term $2.086 \, E(B - V)$ with $E(B - V) = 0.124$ mag (Schlegel et al. 1998), to correct the reddening due to the Galactic dust. Hence, we found the distance modulus $\mu = 25.27 \pm 0.05$ mag. This value is in good agreement with previous estimates (Momany et al. 2002; Weisz et al. 2014; Higgs et al. 2016).

5. SFH from LPV Candidates

The method we employ to determine the SFH, based on the detection of LPV stars, was first introduced and applied successfully to the M33 galaxy by Javadi et al. (2011b). There are also a number of studies that have applied this method (e.g., IC 1613—Hashemi et al. 2018; LMC and SMC—Rezaei kh. et al. 2014; NGC 147 and NGC 185—Hamedani Golshan et al. 2017; M33 galactic disk—Javadi et al. 2017; And I—Saremi et al. 2020; and And VII—Navabi et al. 2021).

In this method, the SFH of a galaxy is defined by the SFR, $\xi(t)$, which is a function of time and describes the amount of star mass formed from gas per year ($M_\odot \, \mathrm{yr}^{-1}$).

$$\xi(t) = \frac{d \, n'(t)}{\delta t} \frac{\int_{min}^{max} f_{IMF}(m)m \, dm}{\int_{m(t)}^{m(t+dt)} f_{IMF}(m) \, dm}, \quad (3)$$

where f_{IMF} is the initial mass function, defined by Kroupa (2001), with the minimum and maximum stellar masses of 0.02 and 200 $M_\odot$. $dn'(t)$ is the number of LPV stars observed in the age bin dt, and δt is the pulsation duration (duration of the evolutionary phase of variability). The numerator shows the

total mass of formed stars, and the denominator is the mass of stars formed in the age bin dt.

To calculate $\xi(t)$, we need to determine the mass, age, and pulsation duration of LPVs. These stars are at the final stage of evolution and have reached maximum brightness. Hence, their luminosity is more directly connected to their birth mass than it is for less evolved stars (Javadi et al. 2011b). To convert the i magnitude to birth mass and estimate δt, we established relations using PARSEC−COLIBRI theoretical stellar isochrones (Marigo et al. 2017), as explained in Saremi et al. (2021). LPVs are assumed to be located at the brightest point of isochrones. For isochrones with a logarithmic age of 6.6–10.16 Gyr, the mass–luminosity relation was determined by fitting the best function to the theoretical i magnitudes over the associated masses. Likewise, the mass–age relation was obtained by fitting the best function to the distribution of masses and ages. Finally, we estimated the pulsation-duration–mass relation by fitting multiple Gaussian functions to the relative pulsation duration over the mass range. Saremi et al. (2021) provide the fits, coefficients, and intercept values of all three relations for different metallicities. We used coefficients and intercepts for SagDIG metallicity after applying the distance modulus and Galactic extinction in line of sight to SagDIG. As shown in Figure 8, due to the dimming caused by circumstellar dust, LPV candidates with a high reddening are fainter than expected. Hence, we applied a correction for all the stars with color $(V - i) > 1.35$ mag. We de-reddened them using the slope of their related isochrones before applying the mass–luminosity relation.

SagDIG's low metallicity has been estimated from RGBs both photometrically ([Fe/H] = −2.1 ± 0.2 dex or Z = 0.00025) by Momany et al. (2002) and spectroscopically ([Fe/H] = $-1.88^{+0.13}_{-0.09}$) by Kirby et al. (2017). The metallicity of H II regions is evaluated to be [Fe/H] = 2.07 ± 0.20 (Saviane et al. 2002), which shows that the interstellar medium is not considerably metal enriched (Momany et al. 2002). However, Momany et al. (2005) showed that a slight enrichment of ∼0.4 dex, compared to the main population of RGBs, is noticeable. Kirby et al. (2017) also showed that the metallicity of stars increases continuously. In this study, we estimated the SFH for three metallicities Z = 0.0002, 0.0003, and 0.0004 ([Fe/H] $\simeq$ −1.7), to account for the chemical enrichment. Figure 12 shows the mass distribution of the LPV candidates for three choices of metallicities. As we expected for the low-mass SagDIG, all LPV candidates have low to intermediate mass.

6. Results and Discussion

6.1. Carbon-rich and Oxygen-rich Stars

With our limited epochs, we are unable to derive the pulsation periods and confirm our LPV candidates. In this section, we compare our list of LPV candidates with other studies that have explored the chemical type and variability of the AGB population in SagDIG. This would confirm some of our LPV candidates. Moreover, as part of the objectives of our survey, we are interested in the dust production of LPVs and its relation to their metallicity.

As a low-mass and low-luminosity galaxy, SagDIG has few C-rich stars (Demers & Battinelli 2002) in comparison to massive galaxies that harbor hundreds (or more) of them. Cook (1987) was the first who attempted to study SagDIG's C-rich stars, and detected 26 C-rich stars employing the narrow-band
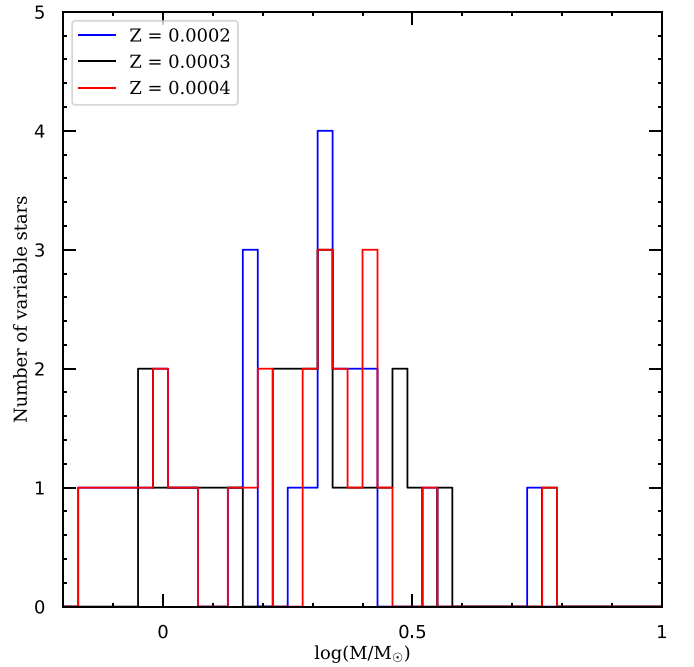
Figure 12. Distribution of stellar masses for three metallicities Z = 0.0002 (in blue), Z = 0.0003 (in black), and Z = 0.0004 (in red). The range of masses shows that all LPV candidates have a low to intermediate mass.

photometry method with filters centered on TiO and CN molecule bands. Demers & Battinelli (2002) applied the same approach and found 16 C-rich stars, eight of which were identified by Cook (1987). For many of Cook's C-rich stars with blue colors, Demers & Battinelli (2002) found small CN −TiO values and ruled them out. We found all of Demers & Battinelli's C-rich stars in our catalog, but we only identified four of them as LPVs. We also found four of Cook's C-rich stars to be LPVs; however, two of them are among Demers & Battinelli's C-rich stars.

Gullieuszik et al. (2007) identified 27 C-rich candidates in SagDIG using broadband photometry in the near-IR. With this approach, more faint and dust-enshrouded C-rich stars can be identified compared to narrow-band photometry. They found six new C-rich stars with $J - K_s > 1.9$ mag and 18 in common with those of Cook (1987) and Demers & Battinelli (2002), which are bluer and mostly have $1.1 < J - K_s < 1.5$ mag. We found 23 of their C-rich stars in our catalog and identified nine as LPVs. In addition, one of the C-rich stars in their list is classified as an LPV based on our estimated variability index, but it is situated at $2.1r_h$ from the center of SagDIG. Moreover, Gullieuszik et al. (2007) classified three C-rich stars in their catalog as LPVs using ACS/HST (Momany et al. 2005) and Demers & Battinelli's photometry. Two of these LPVs are among our LPV candidates and have a very red color.

Momany et al. (2014) investigated the membership of AGB stars in the Cook (1987) and Demers & Battinelli (2002) studies by imposing a threshold on the estimated proper motion of these stars. In total, they found 21 C-rich stars shared by both studies and seven O-rich stars in common with those in Demers & Battinelli (2002). We identified 24 stars from the Momany et al. (2014) list, seven of which are among our LPV candidates. Six of them are C-rich, all with the reddest color.

Figure 13 shows the CMD of our LPV candidates in common with other studies (left panel) and their chemical type (right panel). All of the LPV candidates are in the red part of
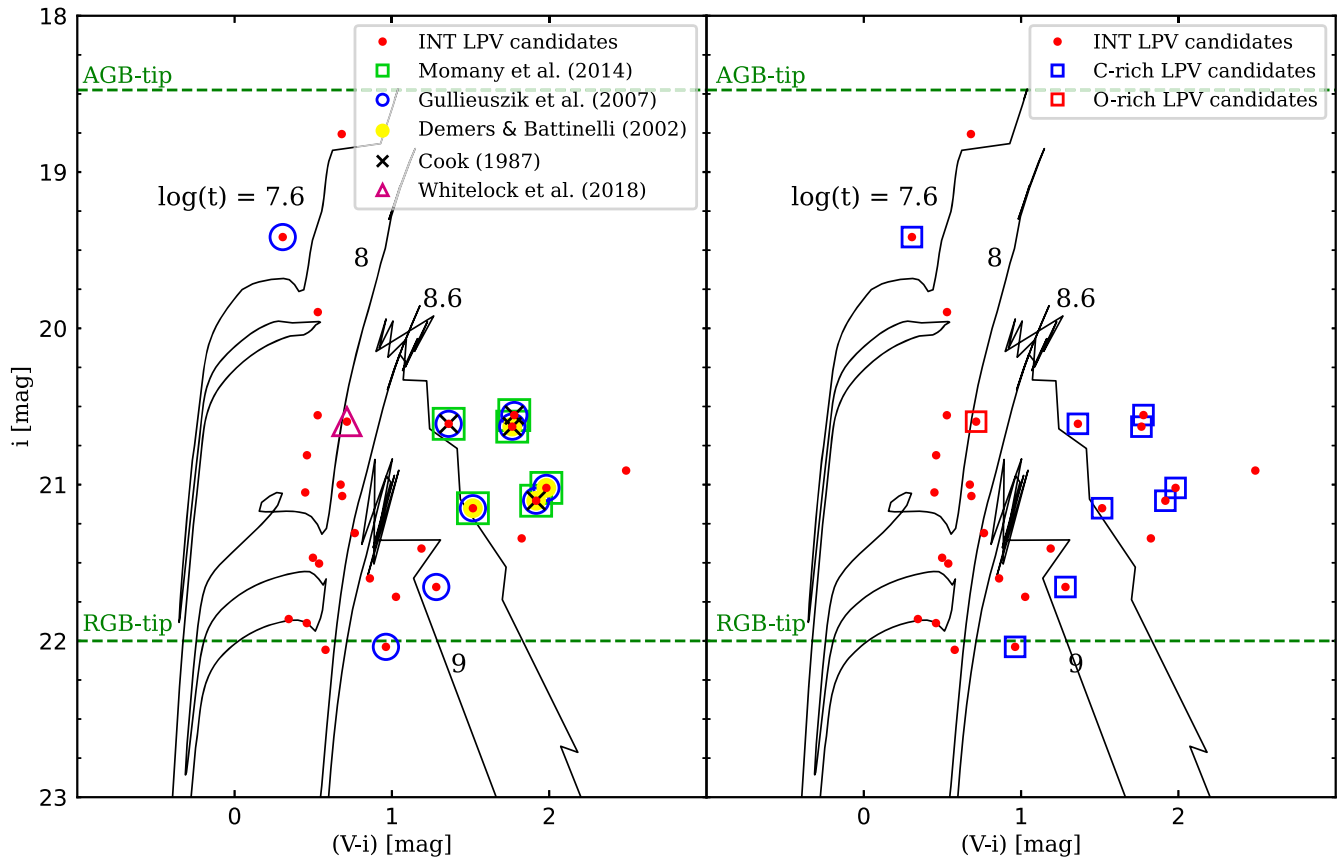
Figure 13. CMD of our LPV candidates (red dots) in the i band vs. $V-i$. Left panel: LPV candidates in common with other studies are shown. Right panel: C-rich and O-rich stars identified in other studies are marked as blue and red squares.

the CMD, and mainly those with the reddest color are C-rich. In general, exploring the chemical type of our LPVs via other studies leads to one O-rich star detection by Whitelock et al. (2018) with a pulsation period of approximately 950 days with a main-sequence mass of 5 $M_\odot$. The period–luminosity (P–L) relation of this star reveals that it undergoes hot bottom burning (HBB).

6.2. x-AGBs and DUSTiNGS Survey

x-AGBs are dusty stars known to be the principal dust producers among thermally pulsating AGBs. Their potentially important role as sources of dust in the first galaxies can be better understood with the help of surveys exploring them in metal-poor galaxies. The DUST in Nearby Galaxies with Spitzer (DUSTiNGS) infrared survey (Boyer et al. 2014) observed 50 galaxies within 1.5 Mpc at 3.6 and 4.5 μm. Their purpose was to map the variable AGBs and statistically study this late stage of evolution and the dust production dependence on the parent galaxy's metallicity.

DUSTiNGS used the constraints (green-dashed line in the left panel Figure 14) that had previously been employed for the Magellanic Clouds with more than 90% accuracy (Boyer et al. 2015) to determine x-AGBs. For SagDIG, which lies in the range of metal-poor galaxies (galaxies with [Fe/H] < −2.0), they found 17 x-AGBs and six variable x-AGBs. SagDIG has the highest number of very metal-poor x-AGBs among other galaxies in their study. Though it has fewer x-AGBs than massive and more metal-rich galaxies, such stars' existence would suggest no correlation between metallicity and dust

production (Boyer et al. 2015). Four of these x-AGBs are classified as C-rich stars in previous studies, one in Demers & Battinelli (2002) and three in Gullieuszik et al. (2007).

In total, we found 397 common sources with the DUSTiNGS catalog within 2r_h of SagDIG. We identified two x-AGBs in our catalog, but only one of them was classified as an LPV candidate in our study. This is not surprising since x-AGBs are very dusty, and in optical photometry, we are solely able to identify those with [3.6] − [4.5] < 0.5 mag. The left panel in Figure 14 shows the CMD in 3.6 and 4.5 μm with the constraints mentioned earlier. Most of our LPVs lie on the log(t) = 8 and 8.6 Gyr isochrones and have [3.6] − [4.5] < 0.5 mag. There are four LPV candidates within the x-AGBs' criterion. The right panel in Figure 14 shows the distribution of LPVs in the i and 3.6 μm CMD. The confirmed x-AGB star (the green square) is faint and dusty.

For further investigation of the chemical types of dusty AGBs in very metal-poor galaxies including SagDIG and DUSTiNGS IV, Boyer et al. (2017) used additional observations from WFC3/IR with F127M, F139M, and F153M filters (best matched to H_2O, CN, and C_2 features). These filters are more efficient than optical narrow-band and near-IR broadband photometry in distinguishing between C-rich and O-rich stars and identifying very faint dust-enshrouded AGBs. For SagDIG, they found 37 AGBs, most of them classified as C-rich stars. We identified six C-rich stars (one of them is the x-AGB from DUSTiNGS II and the others were among C-rich stars in previous studies). They identified two very dusty O-rich stars. We identified both of these stars, but only one of them is among our LPV candidates, which is the same O-rich star as
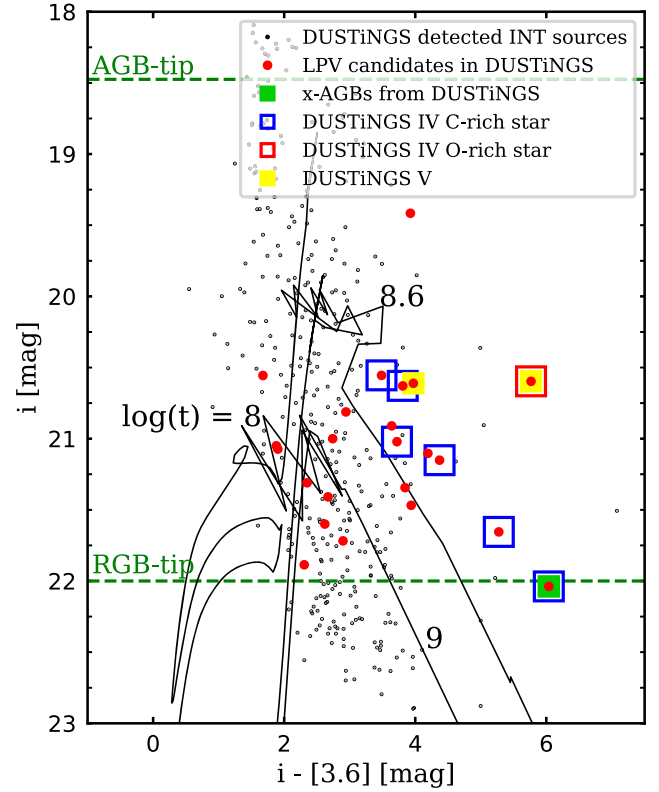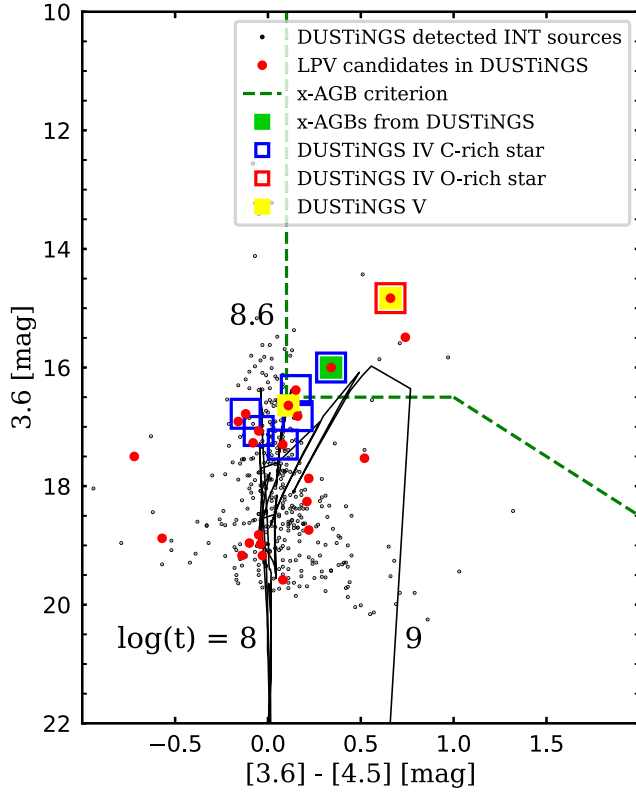
Figure 14. CMD of common sources between DUSTiNGS and our catalog in the [3.6] band vs. [3.6] − [4.5] (left panel) and in the i band vs. i − [3.6] (right panel). In both panels, the red dots represent our LPV candidates. C-rich and O-rich stars from DUSTiNGS are overplotted. The boundary for identifying x-AGBs is shown by the green-dashed line in the left panel.

discovered by Whitelock et al. (2018). As can be seen in Figure 14, the O-rich star (red square) has a large i − [3.6] = 5.8 mag, comparable to the C-rich x-AGB star (green square). This is an indication that, unlike theoretical model predictions for low-metallicity environments, O-rich stars produce a large amount of dust consistent with [3.6] − [4.5] color.

In DUSTiNGs V, Goldman et al. (2019) used extra epochs of observations with the Spitzer telescope to investigate the P–L relation in galaxies with different metallicities. They showed that the P–L relation is unchanged at low metallicity, and the dust production and pulsation are linked as previous studies suggested. They estimated the period of three LPVs in SagDIG. As shown in Figure 14, two of these stars are among our LPV candidates. One of them has a period of 928 days in 3.6 μm and ∼2000 days in 4.5 μm. The other is the most metal-poor O-rich AGB star ever known (the same as Whitelock et al. 2008 found) and is currently experiencing HBB. They estimated the period of the O-rich LPV to be ∼2000 days. Since the estimation was made with insufficient data, the 950 days that Whitelock et al. (2018) estimated are more reliable.

6.3. SFH

To construct the SFH of SagDIG, we defined different age bins consisting of nearly an equal number of LPV candidates to have a uniform uncertainty, and we used the method explained in Section 5. Figure 15 represents the SFR within $2r_{\rm h}$ (0.68 kpc^2) for three metallicities, starting around 13 Gyr ago (log(t [Gyr]) = 10.13) up to 63 Myr ago (log(t[Myr]) = 7.8). The vertical error bars denote SFH errors in each age bin based on Poisson statistics. As shown in Figure 15, SagDIG has had
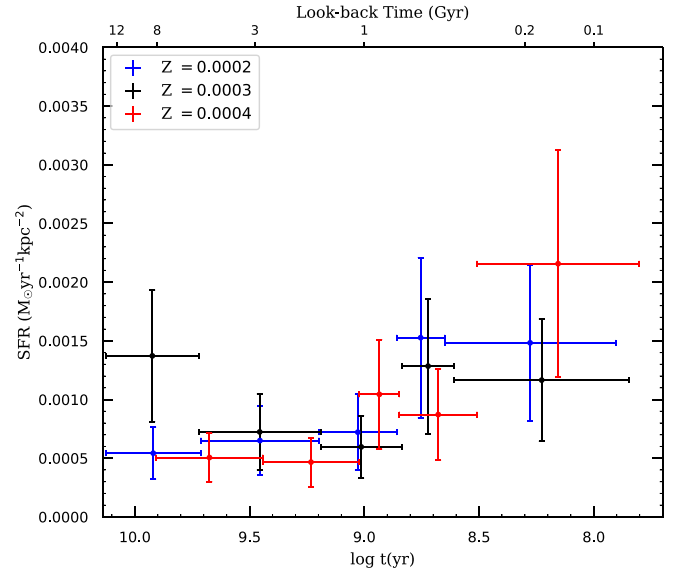
Figure 15. The SFR of SagDIG within $2r_{\rm h}$ for three metallicities $Z = 0.0002$ (in blue), $Z = 0.0003$ (in black), and $Z = 0.0004$ (in red).

continuous star formation activity over its lifetime with different rates and has experienced an enhancement of star formation since ≃1 Gyr ago, which is quite common among dIrr galaxies (Weisz et al. 2014).

Assuming $Z = 0.0002$, SagDIG experiences the lowest SFR ≃0.0005 ± 0.0002 $M_\odot$ yr^{-1} kpc^{-2} around 13 Gyr ago (log(t [Gyr]) = 10.13–9.7). Considering the error bars, the SFR remains nearly constant up to ≃0.6 Gyr ago (log(t[Gyr] ≃ 8.8). Afterward, the SFR increases and its peak reaches

$\simeq 0.0015 \pm 0.0007 \ M_\odot \ \text{yr}^{-1}\text{kpc}^{-2}$ at 0.6–0.08 Gyr ago ($\log(t$ [Gyr]$) \simeq 8.8$–7.9), which is around 3 times higher than SagDIG's lowest SFR. In general, the SFH for all three metallicity choices does not differ considerably, except for the younger population. Assuming $Z = 0.0004$, the peak of SFR increases to $0.0021 \pm 0.0010 \ M_\odot \ \text{yr}^{-1} \ \text{kpc}^{-2}$ and shifts toward younger ages ($\log(t[\text{Gyr}]) \simeq 8.5$–7.8).

Considering the errors, our result is in good accordance with that of Karachentsev et al. (1999). They compared a synthetic CMD to I- and V-band observations from the 2.5 m Nordic Optical Telescope. They estimated the SFR of 0.00028 ± 0.00001 and $0.00144 \pm 0.00017 \ M_\odot \ \text{yr}^{-1} \ \text{kpc}^{-2}$ for the age range of 15–0.2 and 0.2–0.05 Gyr, respectively. We note that we estimated a higher value of SFR at 1–0.2 Gyr ago. However, as Karachentsev et al. (1999) mentioned, their estimation at this interval is uncertain due to poor sampling caused by foreground stars and low star counts in the CMD. They also adopted a metallicity range of $0.0004 < Z < 0.0005$ for the reason that the stellar evolutionary models were incomplete for lower metallicities at that time. Moreover, the considered area in their study was around 0.46 kpc^{-2} and smaller than our field. Momany et al. (2005) estimated the SFR $\simeq 0.00027 \ M_\odot \ \text{yr}^{-1}$ for the last 0.6 Gyr, in a smaller field, using HST/ACS images and the luminosity function of main-sequence stars. Their result was in good agreement with Karachentsev et al. (1999), though, for the last 0.02 Gyr, their estimation is lower and more compatible with H_α flux from Strobel et al. (1991).

Our study only covers SFH up to 63 Myr ago. However, other studies demonstrated the rapidly growing state of SagDIG by tracing blue stars. For example, Hunter et al. (2012) used UV flux from the GALEX survey, and Strobel et al. (1991) and Hunter et al. (2012) used H_α flux of ionized hydrogen from the only H II region in SagDIG. UV flux is a good tracer of the SFR over 100–200 Myr ago, whereas H_α flux only represents the star formation in the past 10 Myr. The estimated SFR in the last age bin in our study is very close to the calculated SFR from far-UV images of the GALEX survey (Hunter et al. 2012). They found $\log\text{SFR}_D^{\text{FUV}} = -2.11 \pm 0.01 \ M_\odot \ \text{yr}^{-1} \ \text{kpc}^{-2}$. The value is scaled to the area with disk scale length $R_D = 0.23 \pm 0.03$ kpc. By multiplying the area, the SFR is equal to $0.0013 \ M_\odot \ \text{yr}^{-1}$, which is close to our estimation for the latest age interval.

For $Z = 0.0002$, 0.0003, and 0.0004 we estimated the total stellar mass $M_*(< 2r_h) = (5.4 \pm 2.3) \times 10^6 \ M_\odot$, $(9.6 \pm 4.0) \times 10^6 \ M_\odot$, and $(3.0 \pm 1.3) \times 10^6 \ M_\odot$, respectively. This is in good agreement with previous estimates. McConnachie (2012) determined $M_* = 3.5 \times 10^6 \ M_\odot$ with the assumption of a stellar mass-to-light ratio of 1. Young & Lo (1997) estimated $(2.5$–$7.5) \times 10^6 \ M_\odot$, assuming a stellar mass-to-light ratio of 1–3.

To further study the amount of formed mass in different epochs, we defined the cumulative SFH as the fraction of stellar mass formed as a function of look-back time. To better compare our results with those of Weisz et al. (2014), who used HST deep images to obtain the cumulative SFH of LG dwarf galaxies, we overlay their measured SFH in Figure 16. They found that, like most dIrrs, SagDIG underwent an increase in star formation since $z = 1$. We also found an increase in the SFH since $z \simeq 1$ ($\log(t[\text{Gyr}]) \simeq 8.8$–9.0), though it is more noticeable in Figure 15. As shown in Figure 16, our results imply that SagDIG formed only 30% of its total stellar mass
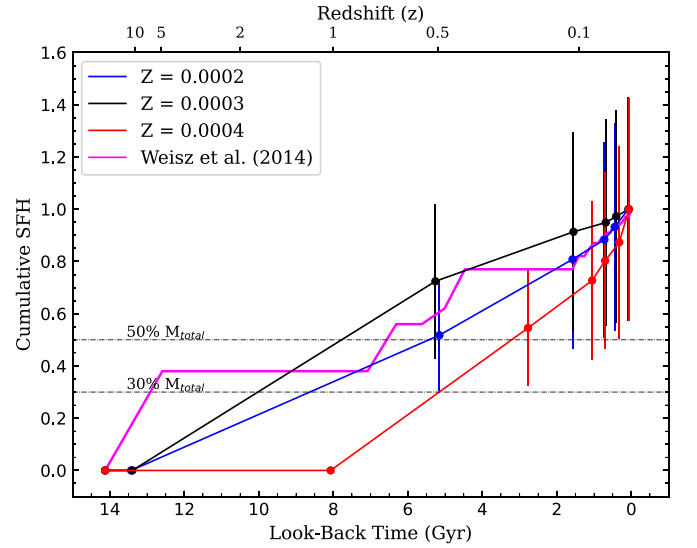
Figure 16. Cumulative SFH of SagDIG within $2r_h$ for three metallicities $Z = 0.0002$ (in blue), $Z = 0.0003$ (in black), and $Z = 0.0004$ (in red). The black-dashed lines represent 30% and 50% of the total stellar mass formed. The cumulative SFH from Weisz et al. (2014) is overlaid to compare.
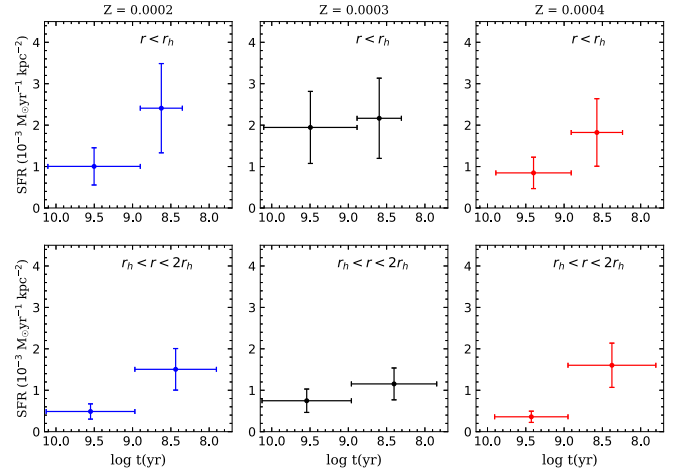
Figure 17. The SFR of SagDIG for three metallicities $Z = 0.0002$, 0.0003, and 0.0004 inside r_h and within r_h–$2r_h$.

prior to $\simeq 8.5$ Gyr ago ($z = 1.2$), and the fraction increased to about 50% by 5 Gyr ago. Weisz et al. (2014) estimated that 30% of SagDIG's stellar mass formed before $z = 2$ (10.5 Gyr ago), and around 50% formed before 6 Gyr ago and concluded the latter as the mean age of SagDIG.

6.4. Spatial Distribution and Age Gradient

To investigate the age gradient in SagDIG, we divided the LPV candidates into two groups based on their distance from the galaxy center. We estimated the ratio of SFR in older times ($\log t(\text{yr}) > 9.2$, $Z = 0.0002$) to that of more recent times ($\log t(\text{yr}) < 9$, $Z = 0.0004$), for both $r < r_h$ and $r_h < r < 2r_h$, to be 0.56 and 0.31, respectively. Considering the errors (minimum of the old SFR and maximum of the recent SFR), the ratios become 0.23 and 0.15. The slightly higher ratio of SFR in the inner region and the extension of SFR to more recent times in the outer part, as shown in Figure 17, could suggest an inside-out formation scenario by internal or external processes. However, the difference in the ratio of SFR between

the two regions is not significant enough to strongly confirm this scenario. Moreover, considering the isolation of SagDIG, any external interaction or merger with another galaxy is highly unlikely.

The evolution of dwarf galaxies is susceptible to their environment. Although SagDIG is an isolated galaxy today, could it have experienced some interactions in the past that would have caused the spatial extension of the intermediate-age population? Our analysis here is limited to $2'.2$. Therefore, any deduction from our results about the structure and the possibility of tidal interactions might not be robust. Nevertheless, the extended structure of SagDIG has been studied out to $5'$ (Beccari et al. 2014), and beyond that (Higgs et al. 2016), suggesting the possibility of tidal interaction in the past. SagDIG's H I has a distributed morphology and a large gradient in the kinematics, though with no sign of rotation. Aside from possible internal processes, Beccari et al. (2014) stated that tidal interaction may have played a role in the characteristics of H I. Higgs et al. (2016) found a mild distortion in RGB distribution in the exterior part of SagDIG along the major axis. They speculated that this is a sign of tidal interaction in the past with a small object like a globular cluster. However, they also offered another explanation and found it more likely: SagDIG has a secondary component that encompasses the main body, such as a stellar halo that extends beyond $5'$.

By investigating the spatial distribution of the intermediate-age and old populations, McQuinn et al. (2017) found that in SagDIG, TP-AGBs have a longer scale length in comparison to RGBs. They also found breaks in the RGB and AGB surface density at $\lesssim 3'$, where the H I column density also decreases. They concluded that their findings, in addition to the distributed morphology and the kinematics of H I, suggest that SagDIG has undergone tidal interactions Considering the tidal scenario and the uncertain durability of tidal interaction in a low-mass system, the current position of the intermediate-age population does not reflect the formation scenario of these populations, i.e., whether they were pulled out after formation or formed in the outer extremities at the first place (McQuinn et al. 2017).

7. Summary and Conclusions

This paper presented the SFH of the SagDIG galaxy based on detecting LPVs in i- and V-band observations taken during 2016–2017 with the Isaac Newton Telescope. 27 LPV candidates were detected within 2 half-light radii of SagDIG; 10 were in common with other studies, including nine C-rich stars and one O-rich star. Considering a slight metallicity enrichment $(Z = 0.0004)$, we estimated the SFR of 0.0021 ± 0.0010 $M_\odot$ yr^{-1} kpc^{-2} at 0.3–0.06 Gyr ago (log(t [Gyr]) $\simeq 8.5$–7.8), which is $\simeq 4$ times higher than the lowest SFR in older ages with $Z = 0.0002$. Moreover, SagDIG assembled 30% and 50% of its stellar mass prior to 8.5 and 5 Gyr ago, respectively. SagDIG has had continuous star formation, and like many dIrrs, its SFR has increased since $z \simeq 1$. The total stellar mass within $2r_\mathrm{h}$ from the center of SagDIG was estimated for three different choices of metallicity. For $Z = 0.0002$ and 0.0004, we estimated the stellar mass $(5.4 \pm 2.3) \times 10^6$ and $(3.0 \pm 1.3) \times 10^6$ $M_\odot$, respectively. We also determined a distance modulus of $\mu = 25.27 \pm 0.05$ mag using the TRGB method.

ORCID iDs

Atefeh Javadi ⓘ https://orcid.org/0000-0001-8392-6754
Elham Saremi ⓘ https://orcid.org/0000-0002-5075-1764
Jacco Th. van Loon ⓘ https://orcid.org/0000-0002-1272-3017
Mahdieh Navabi ⓘ https://orcid.org/0000-0001-9438-5228

References

Beccari, G., Bellazzini, M., Fraternali, F., et al. 2014, A&A, 570, A78
Boyer, M. L., McQuinn, K. B. W., Barmby, P., et al. 2014, ApJS, 216, 10
Boyer, M. L., McQuinn, K. B. W., Barmby, P., et al. 2015, ApJ, 800, 51
Boyer, M. L., McQuinn, K. B. W., Groenewegen, M. A. T., et al. 2017, ApJ, 851, 152
Cesarsky, D. A., Laustsen, S., Lequeux, J., Schuster, H. E., & West, R. M. 1978, A&A, 65, 153
Chambers, K. C., Magnier, E. A., Metcalfe, N., et al. 2016, arXiv:1612.05560
Cook, K. H. 1987, PhD thesis, Univ. of Arizona
Demers, S., & Battinelli, P. 2002, AJ, 123, 238
Erben, T., Schirmer, M., Dietrich, J. P., et al. 2005, AN, 326, 432
Gaia Collaboration, Brown, A. G. A., Vallenari, A., et al. 2021, A&A, 649, A1
Girardi, L., Groenewegen, M. A. T., Hatziminaoglou, E., & da Costa, L. 2005, A&A, 436, 895
Goldman, S. R., Boyer, M. L., McQuinn, K. B. W., et al. 2019, ApJ, 877, 49
Gullieuszik, M., Rejkuba, M., Cioni, M. R., Habing, H. J., & Held, E. V. 2007, A&A, 475, 467
Hamedani Golshan, R., Javadi, A., van Loon, J. T., Khosroshahi, H., & Saremi, E. 2017, MNRAS, 466, 1764
Hashemi, S. A., Javadi, A., & van Loon, J. T. 2018, MNRAS, 483, 4751
Haynes, M. P. 2019, in IAU Symp. 344, Dwarf Galaxies: From the Deep Universe to the Present, ed. K. B. W. McQuinn & S. Stierwalt (Cambridge: Cambridge Univ. Press), 3
Higgs, C. R., McConnachie, A. W., Irwin, M., et al. 2016, MNRAS, 458, 1678
Hunter, D. A., Ficut-Vicas, D., Ashley, T., et al. 2012, AJ, 144, 134
Javadi, A., van Loon, J. T., Khosroshahi, H. G., et al. 2017, MNRAS, 464, 2103
Javadi, A., van Loon, J. T., & Mirtorabi, M. T. 2011a, MNRAS, 411, 263
Javadi, A., van Loon, J. T., & Mirtorabi, M. T. 2011b, MNRAS, 414, 3394
Karachentsev, I., Aparicio, A., & Makarova, L. 1999, A&A, 352, 363
Kirby, E. N., Rizzi, L., Held, E. V., et al. 2017, ApJ, 834, 9
Kroupa, P. 2001, MNRAS, 322, 231
Landolt, A. U. 1992, AJ, 104, 340
Lee, M. G., Freedman, W. L., & Madore, B. F. 1993, ApJ, 417, 553
Longmore, A. J., Hawarden, T. G., Webster, B. L., Goss, W. M., & Mebold, U. 1978, MNRAS, 183, 97P
Marigo, P., Girardi, L., Bressan, A., et al. 2017, ApJ, 835, 77
McConnachie, A. W. 2012, AJ, 144, 4
McQuinn, K. B. W., Boyer, M. L., Mitchell, M. B., et al. 2017, ApJ, 834, 78
Momany, Y., Held, E. V., Saviane, I., & Rizzi, L. 2002, A&A, 384, 393
Momany, Y., Held, E. V., Saviane, I., et al. 2005, A&A, 439, 111
Momany, Y., Clemens, M., Bedin, L. R., et al. 2014, A&A, 572, A42
Navabi, M., Saremi, E., Javadi, A., et al. 2021, ApJ, 910, 127
Parto, T., Dehghani, S., Javadi, A., et al. 2021, arXiv:2101.10874
Rezaei kh., S., Javadi, A., Khosroshahi, H., & van Loon, J. T. 2014, MNRAS, 445, 2214
Sakai, S., Madore, B. F., & Freedman, W. L. 1996, ApJ, 461, 713
Saremi, E., Javadi, A., Navabi, M., et al. 2021, ApJ, 923, 164
Saremi, E., Javadi, A., van Loon, J. T., et al. 2017, JPhCS, 869, 012068
Saremi, E., Javadi, A., Th. van Loon, J., et al. 2020, ApJ, 894, 135
Saviane, I., Rizzi, L., Held, E. V., Bresolin, F., & Momany, Y. 2002, A&A, 390, 59

Schlegel, D. J., Finkbeiner, D. P., & Davis, M. 1998, ApJ, 500, 525
Simon, J. D. 2019, ARA&A, 57, 375
Stetson, P. B. 1987, PASP, 99, 191
Stetson, P. B. 1990, PASP, 102, 932
Stetson, P. B. 1993, in IAU Colloq. 136, Stellar Photometry: Current Techniques and Future Developments, ed. C. J. Butler & I. Elliott (Cambridge: Cambridge Univ. Press), 291

Stetson, P. B. 1994, PASP, 106, 250
Stetson, P. B. 1996, PASP, 108, 851
Strobel, N. V., Hodge, P., & Kennicutt, R. C., Jr. 1991, ApJ, 383, 148
Weisz, D. R., Dolphin, A. E., Skillman, E. D., et al. 2014, ApJ, 789, 147
Whitelock, P. A., Menzies, J. W., Feast, M. W., & Marigo, P. 2018, MNRAS, 473, 173
Young, L. M., & Lo, K. Y. 1997, ApJ, 490, 710